RSC Advances

ROYAL SOCIETY OF CHEMISTRY

www.rsc.org/advances

RSC Advances

RSCPublishing

ARTICLE

A facile synthetic approach for SiO_2@Co_3O_4 core–shell nanorattles with enhanced peroxidase–like activity

Cite this: DOI: 10.1039/x0xx00000x

Syam Kandula and Pethaiyan Jeevanandam*

Received 00th January 2014,
Accepted 00th January 2014

DOI: 10.1039/x0xx00000x

www.rsc.org/

SiO_2@Co_3O_4 core–shell nanorattles with different Co_3O_4 shell thickness have been successfully synthesized by the calcination of SiO_2@α-$Co(OH)_2$ at 500 °C. The synthetic approach is facile, economical, and requires no surface modification. The synthesized materials were thoroughly characterized using powder X–ray diffraction (XRD), Fourier transform infrared spectroscopy (FT–IR), thermal gravimetric analysis (TGA), Brunauer–Emmett–Teller (BET) analysis, field emission scanning electron microscopy (FE–SEM), transmission electron microscopy (TEM), and diffuse reflectance spectroscopy (DRS). SEM analysis indicates hierarchical core–shell morphology for SiO_2@Co_3O_4 and the TEM results indicate the core–shell nanorattle morphology. Diffuse reflectance spectroscopy studies indicate that the SiO_2@Co_3O_4 core–shell nanorattles show two absorption bands in the range 420–450 nm and 700–750 nm related to ligand to metal charge transfer transitions ($O^{2-} \rightarrow Co^{2+}$ and $O^{2-} \rightarrow Co^{3+}$). The SiO_2@Co_3O_4 core–shell nanorattles act as an artificial peroxidase enzyme mimic with enhanced intrinsic peroxidase–like activity compared to pure Co_3O_4 nanoparticles and horseradish peroxidase (HRP), a natural enzyme. The SiO_2@Co_3O_4 core–shell nanorattles show higher k_{cat} and k_{cat}/K_m values compared to pure Co_3O_4 and HRP indicating their applicability as artificial enzyme mimic in biomedicine and bio–sensing.

1. Introduction

In recent times, scientists are paying increasing attention towards the use of metal oxide nanoparticles in various biological applications due to their versatility, sensitivity, stability, etc.[1-6] Enzymes are typically proteins that catalyze bio-chemical reactions in the cellular metabolic processes and they enhance rate of the reactions.[7,8] Horseradish peroxidase (HRP) is a natural peroxidase enzyme which is extracted from plants and it catalyzes decomposition of peroxides and oxidation of various substrates.[9] HRP is expensive, difficult to store, and it easily becomes inactive. Scientists have an immense interest to develop artificial enzymes (mimics) due to the inherent drawbacks of natural enzymes; they have a tendency to undergo denaturation under environmental conditions with low stability, and low redox activity.[7,10] Nanomaterials based enzyme mimics have the advantage of higher stability under harsh conditions, low cost, tunable catalytic activity and they can be potentially useful in different fields of biology.

Silica is chemically inert, stable at elevated temperatures and optically transparent. It is useful in many areas such as glass industries, ceramics, semiconductors, photovoltaic cells and it is also used as catalytic support.[11-13] Co_3O_4 is an important p-type antiferromagnetic semiconductor with a normal spinel structure.[14] It is used in various applications such as anode materials in lithium ion rechargeable batteries,[15] sensors,[16] electrochemical devices,[17] solar energy absorbers,[18] supercapacitors,[19] water oxidation,[20] and heterogeneous catalysis.[21]

In recent years, research is focused on core–shell nanoparticles with yolk–shell or nanorattle morphology. Nanorattles refer to hollow shells with solid cores with interstitial hollow space between the core and the shell. They have a large number of applications in bio–sensing, energy storage, catalysis and biomedicine.[22-25] Nanorattles exhibit interesting characteristics which are useful in multi–functional areas. One of the most explored applications of these materials is their use as nanocatalysts. Up to now, several methods have been reported for the synthesis of nanorattles and they include hydrothermal synthesis, selective etching, template–route, annealing, and Ostwald ripening.[23-28] Tan et al. have reported the synthesis of Au-Pd@SiO_2 nanorattles useful in Suzuki cross-coupling reaction.[23] Yang et al. have reported the

preparation of Fe_3O_4@air@poly(vinylsilane) nanorattles and they have used them as contrast agents.[24] Zhang et al. have reported the preparation of Au@polyanline yolk–shell nanorattles and have used them as flexible memory device.[25] Xu et al. have reported the synthesis of Fe_3O_4@$CuSiO_3$ nanorattles and have investigated their microwave absorption properties.[29] In some cases, Co_3O_4 has been used as the core material and SiO_2 has been used as the shell.[22,30-32] Zong et al. have reported the confined growth of metal oxide nanocrystals on mesoporous silica spheres which act as the core material.[33]

Very less attention has been paid towards the use of metal oxide nanoparticles in biological applications. For example, Mu et al. have reported the peroxidase–like activity for Co_3O_4 nanoparticles and, recently, they have also studied the effect of crystal plane of Co_3O_4 on the peroxidase–like activity.[10,34] Gao et al. have reported that Fe_3O_4 nanoparticles possess intrinsic peroxidase–like activity.[35] In addition to Fe_3O_4 and Co_3O_4 nanoparticles, other systems such as graphene supported Au–Pd bimetallic core–shell nanoparticles,[36] Au nanoparticles on citrate–functionalized graphene sheets,[37] Co–Al layered double hydroxides,[38] porous platinum nanotubes,[39] CuS–graphene nanosheets,[40] and Fe_3O_4 nanoparticles loaded on graphene oxide–dispersed carbon nanotubes[41] have been explored for the intrinsic peroxidase–like activity. Peroxidase–like activity has also been demonstrated in Co_3O_4 nanoparticles coupled with carbon nitride nanotubes and reduced graphene oxide.[42,43] In the present study, SiO_2@Co_3O_4 core–shell nanorattles with uniform Co_3O_4 porous shell over the silica core have been successfully synthesized using a self–template route by the calcination of SiO_2@α-$Co(OH)_2$ at 500 °C. The synthesized materials were thoroughly characterized before examining the intrinsic peroxidase–like activity using 3,3',5,5'-tetramethyl benzidine (TMB) as the substrate.

2. Experimental

2.1 Reagents

Tetraethyl orthosilicate (98%, ACROS®), ethanol (99.9%, AR), ammonia solution (25%, Rankem, AR), cobaltous nitrate hexahydrate (98%, Rankem, LR), urea (99.5%, Rankem, AR) and hydrogen peroxide (30%, Rankem, AR) were used as received without further purification. The peroxidase substrate, 3,3',5,5'–tetramethyl benzidine (TMB), was received from Spectrochem chemicals, India.

2.2 Synthesis

The SiO_2@Co_3O_4 core–shell nanorattles were synthesized in two steps and the procedure is as follows.

2.2.1 Synthesis of silica spheres

Silica microspheres were synthesized according to a previous report.[44] In brief, 88 mL of ethanol was mixed with 12 mL of ammonia solution and 3.7 mL of tetraethyl orthosilicate was added drop wise under vigorous stirring. The contents were continuously stirred at room temperature for 24 h. After completion of the reaction, the contents were centrifuged, washed with ethanol several times and finally dried in an oven for overnight at 80 °C.

2.2.2 Synthesis of SiO_2@Co_3O_4 core–shell nanorattles

About 100 mg each of silica spheres was dispersed in 100 mL of aqueous cobaltous nitrate solution with different concentrations (5 mM, 10 mM and 15 mM) in a 250 mL beaker and sonicated for 3 min. After uniform dispersion of the silica spheres, 5 gm of urea was added. The contents were heated at 85 °C and stirred for 6 h. During the reaction, the color of the contents changed from pink to violet indicating the formation of α–cobalt hydroxide. After 6 h, the contents were allowed to cool to room temperature, filtered using Whatman® filter paper, washed with Millipore® water several times and dried in the oven for overnight. The obtained products were calcined in a muffle furnace (Nabertherm®) at 500 °C for 3 hours (heating rate = 2°/min), under air, to get the SiO_2@Co_3O_4 core–shell nanorattles. The obtained SiO_2@Co_3O_4 samples were labelled as S1, S2, and S3, corresponding to 5 mM, 10 mM and 15 mM concentrations of cobaltous nitrate used during the preparation of SiO_2@α-$Co(OH)_2$ samples, respectively.

2.3 Characterization

Structural analysis of the synthesized samples was carried out using powder X–ray diffraction on a Brucker AXS D8 diffractometer over the 2θ range of 5–85° and the scan rate was 1°/min. Copper was used as the target (Cu–K_α ; λ=1.5406 Å). FT–IR spectral analysis of the samples was carried out on a Thermo Nicolet Nexus FT–IR spectrometer in the range 400–4000 cm^{-1} using KBr pellet method. Thermogravimetric analysis of the as prepared samples were recorded on a EXSTAR TG/DTA 6300 instrument, under air, over the temperature range 25–1000 °C and the heating rate was 10 °/min. Morphological studies of the samples were carried out using a FEI Quanta 200F field emission scanning electron microscope (FE–SEM) operating at 15 kV. Elemental analysis was carried out using an energy dispersive X–ray analysis facility coupled with the FE–SEM instrument. Transmission electron microscopy (TEM) images and selected area electron diffraction (SAED) patterns were obtained using a FEI TECNAI G^2 transmission electron microscope. For the TEM analysis, the sample powders were dispersed in ethanol and sonicated for about 15 mins. Then, one drop each of the suspensions was put on a carbon coated copper grid and allowed to dry in air. Diffuse reflectance spectroscopy (DRS) analysis was carried out on a Shimadzu UV–2450 UV–Visible spectrophotometer using the powder samples in the wavelength range 360 nm–800 nm and $BaSO_4$ (Aldrich) was used as the

reference. Specific surface area of the SiO_2@Co_3O_4 samples was obtained by the Brunauer–Emmett–Teller (BET) method using N_2 adsorption at 77 K on a Nova 2200 e Quantachrome instrument.

2.4 Peroxidase–like redox activity and steady state kinetic analysis

To investigate the peroxidase–like redox catalytic activity of the SiO_2@Co_3O_4 core–shell nanorattles, the oxidation of 3,3',5,5'–tetramethyl benzidine (TMB) was examined in the presence of H_2O_2. The reaction was studied at room temperature in acetic acid–acetate buffer containing SiO_2@Co_3O_4 nanorattles as the catalyst. First, 30 μg of SiO_2@Co_3O_4 catalyst was dispersed in 3 mL of 0.1 M acetate buffer and sonicated for 3 minutes. Then, 300 μL of 3 mM DMSO solution of TMB and 31 μL of 30 % H_2O_2 (100 mM) were added and the absorbance values at λ_{max} = 652 nm were recorded upto 5 minutes in time course mode on a Shimadzu UV–2450 UV-Vis spectrophotometer. Kinetic studies were carried out using the same instrument. While keeping the TMB concentration constant, kinetic analysis was performed by varying the amount of the SiO_2@Co_3O_4 catalyst (5–60 μg per 3 mL), pH of the buffer (2–12), temperature (20–70 °C), and H_2O_2 concentration (5–200 mM). Kinetic studies were also carried out under the following conditions; 30 μg catalyst per 3 mL, pH = 5, temperature = 30 °C and TMB concentration = 0.015–0.4 mM while keeping H_2O_2 concentration as 100 mM. In another kinetic experiment, while keeping the concentration of TMB as 0.3 mM, the concentration of H_2O_2 was varied (20–200 mM). The apparent rate constant values (k_{app}) were evaluated from the absorbance data.[9,10] The Michaelis–Menten constant (K_m) and the maximal reaction rate (V_{max}) were determined from the Lineweaver–Burk double reciprocal plots. The Michaelis–Menten equation can be expressed as

$$1/v = (K_m/V_{max}).(1/[S])+1/V_{max}$$

Where, v is the initial velocity, K_m is the Michaelis–Menten constant, V_{max} is the maximal reaction velocity, and [S] is the concentration of the substrate (TMB).

3. Results and discussion

3.1 Material characterization

Figure 1(a) shows the XRD patterns of as prepared SiO_2, α-$Co(OH)_2$, and SiO_2@α-$Co(OH)_2$. Silica is amorphous. All the XRD patterns show raising background which is attributed to X–ray fluorescence since Cu–K_α was used as the X–ray source during the measurements. The α-$Co(OH)_2$ shows reflections at 12.18°, 24.37°, 33.11°, 38.08°, 45.98°, 52.05°, and 59.71° which are attributed to (003), (006), (012), (015), (018), (100), and (110) crystal planes (JCPDS file no: 46–0605), respectively.[45,46] The first two planes in the XRD pattern of α–$Co(OH)_2$ are related to d–spacing between the intercalated layers ($d_{(003)}$ = $2d_{(006)}$).[47] The XRD patterns of SiO_2@α-$Co(OH)_2$ samples show broad peaks of (003), (006), and (110) planes of α–$Co(OH)_2$ with low crystallinity.[48,49] The interplanar spacings of α–$Co(OH)_2$ and SiO_2@α–$Co(OH)_2$ samples was calculated using the (003) plane and the value is *ca.* 7.2 Å.

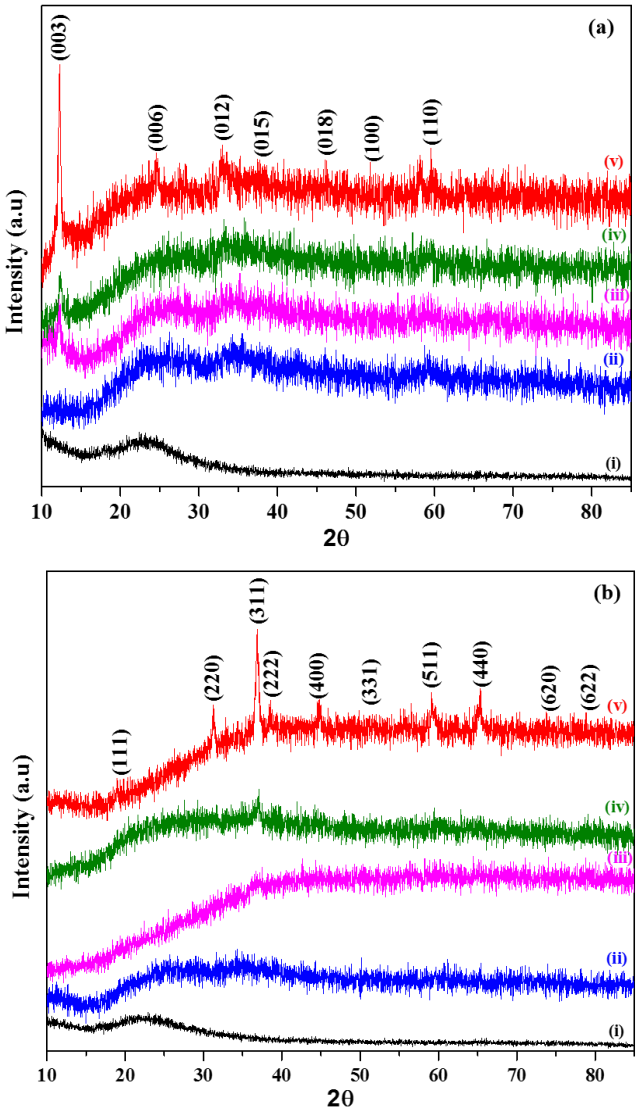

Fig. 1 (a) XRD patterns of (i) as prepared SiO_2, (ii–iv) SiO_2@α-$Co(OH)_2$ samples, and (v) α-$Co(OH)_2$ samples (b) XRD patterns of (i) SiO_2, (ii–iv) SiO_2@Co_3O_4 (S1, S2, and S3), and (v) Co_3O_4. All the samples were calcined at 500 °C.

Figure 1(b) shows the XRD patterns of SiO_2, Co_3O_4 and SiO_2@Co_3O_4 samples (S1, S2, and S3) after calcination at 500 °C. Pure Co_3O_4 shows reflections at 19.09°, 31.26°, 36.89°, 38.47°, 44.77°, 59.19°, 65.27°, 74.26°, and 78.80° corresponding to (111), (220), (311), (222), (400), (511), (440), (620), and (622) planes of cubic Co_3O_4 (JCPDS file no: 42–1467), respectively. Since the major component in the core-shell nanorattles is SiO_2 which is amorphous, the XRD patterns for SiO_2@α–$Co(OH)_2$ as well as SiO_2@Co_3O_4 core-shell

nanorattles (obtained on calcination) indicate poorly crystallinity. The XRD patterns for α–$Co(OH)_2$ (Figure 1a (v)) and pure Co_3O_4 (Figure 1b (v)), however, show that these samples are more crystalline compared to the other samples. Calcination does not improve the crystallinity since it only converts α–$Co(OH)_2$ present on SiO_2 to Co_3O_4 and Co_3O_4 exists as small nanoparticles (as evidenced by the TEM results). XRD results indicate the formation of α-$Co(OH)_2$ on SiO_2 spheres. On calcination at 500 °C, the formation of Co_3O_4 nanoparticles on SiO_2 is evident.

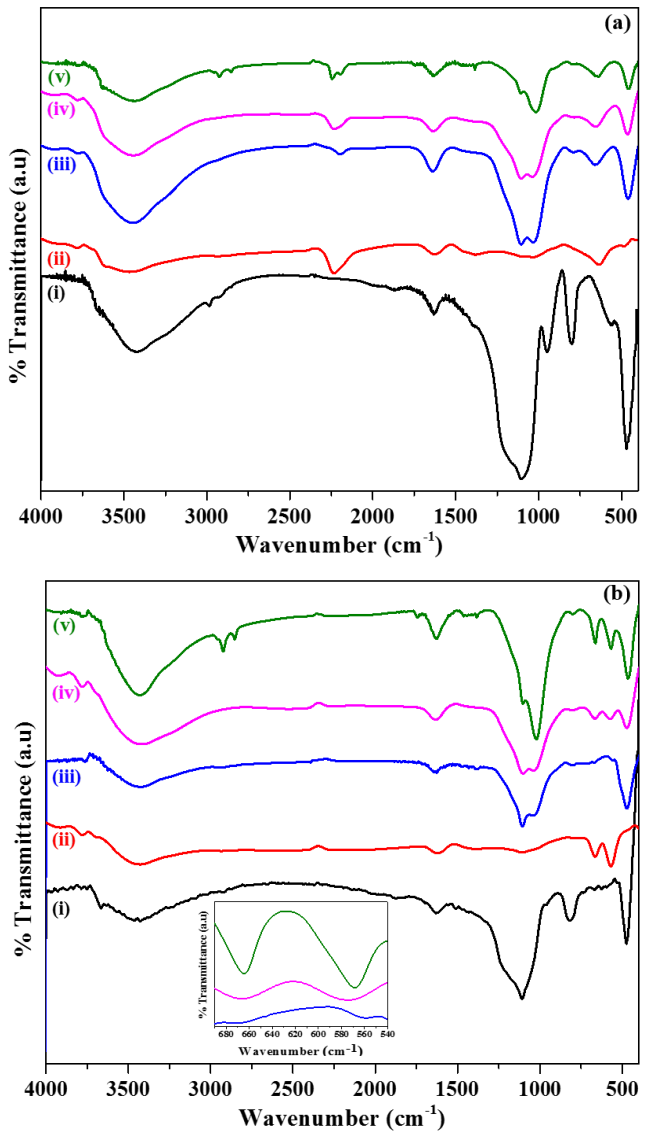

Fig. 2 (a) FT–IR spectra of (i) as prepared SiO_2, (ii) α-$Co(OH)_2$, (iii–v) SiO_2@α-$Co(OH)_2$ and (b) FT–IR spectra of (i) SiO_2, (ii) Co_3O_4, and (iii–v) SiO_2@Co_3O_4 (S1, S2, and S3) samples after calcination at 500 °C. The inset shows the magnified view of IR bands for SiO_2@Co_3O_4 samples (S1, S2, and S3).

FT–IR spectra were recorded for as prepared SiO_2, α-$Co(OH)_2$, and SiO_2@α-$Co(OH)_2$ (Figure 2a). The IR spectra for calcined SiO_2, Co_3O_4, SiO_2@Co_3O_4 (S1, S2, and S3) samples are shown in Figure 2b. All the samples show two bands at about 3430 cm^{-1} and 1630 cm^{-1} assigned to stretching and bending vibrations of –OH groups of surface physisorbed water molecules. All the samples except the α–$Co(OH)_2$ and Co_3O_4 show bands at about 1100 cm^{-1}, 800 cm^{-1}, and 475 cm^{-1} attributed to asymmetric, symmetric stretching, and bending vibration modes of Si–O–Si. Pure SiO_2 shows a characteristic band at 950 cm^{-1} due to Si–OH group.[44] The SiO_2@α-$Co(OH)_2$ samples and α-$Co(OH)_2$ show IR bands at 2235 cm^{-1}, and 1387 cm^{-1}, attributed to the stretching frequencies of NCO^-, and NO_3^-, respectively. This indicates the presence of NCO^- and NO_3^- in between the layers.[47,50] All the samples except SiO_2 show a band at 1023 cm^{-1} attributed to the deformation mode of –OH group.[51] The α-$Co(OH)_2$ and SiO_2@α-$Co(OH)_2$ samples show a band at about 660 cm^{-1} attributed to Co–OH vibration. Pure Co_3O_4 shows two characteristic bands attributed to Co(II)–O stretching when Co^{2+} ions are in tetrahedral coordination and Co(III)–O stretching when Co^{3+} ions are in octahedral coordination;[50] SiO_2@Co_3O_4 (S1) shows IR bands at 667 cm^{-1} and 560 cm^{-1}, sample S2 shows bands at 667 cm^{-1} and 576 cm^{-1}, and sample S3 shows bands at 664 cm^{-1} and 568 cm^{-1}. In summary, FT–IR results show the evidence for the presence of NCO^- and NO_3^- ions in α-$Co(OH)_2$, and SiO_2@α-$Co(OH)_2$ and the presence of Co_3O_4 in the SiO_2@Co_3O_4 samples.

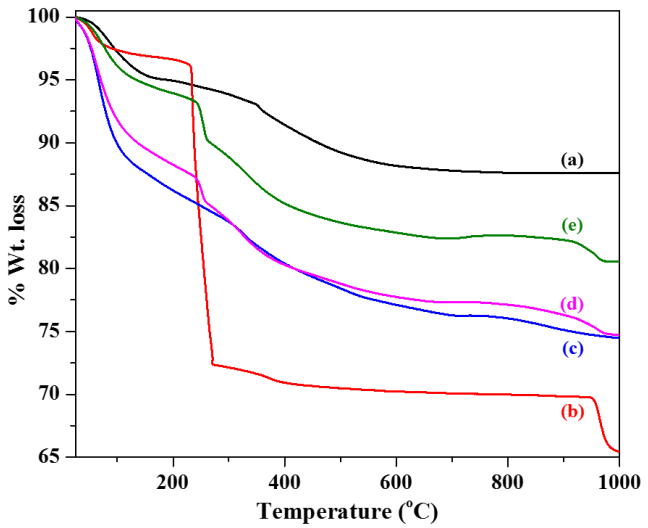

Fig. 3 TGA patterns of (a) as prepared SiO_2, (b) α-$Co(OH)_2$, and (c–e) SiO_2@α-$Co(OH)_2$ samples.

The thermogravimetric analysis (TGA) patterns of as prepared SiO_2, α-$Co(OH)_2$, and SiO_2@α-$Co(OH)_2$ samples are shown in Figure 3. The as prepared SiO_2 shows a total weight loss of 12.5 % upto 1000 °C with two weight loss steps. The first step from 35 °C to 170 °C (weight loss = 5 %) is attributed to the loss of physisorbed water molecules. The second weight loss from 350 °C to 660 °C (wt. loss = ~ 7.5 %) is attributed to the dehydroxylation of surface hydroxyl groups.[52] The α–$Co(OH)_2$ shows a total weight loss of about 35 % upto 1000 °C in three steps. The weight loss upto 150 °C (~ 2.5 %) is related to the loss of surface physisorbed water molecules. The major weight loss (~ 28.3 %) observed between 220 and 400 °C is attributed to the loss of intercalated water molecules, anions,

and dehydroxylation of α–$Co(OH)_2$ accompanied by its conversion to spinel Co_3O_4.[53] Another weight loss (~ 4.2 %) between 940 and 985 °C is associated with the thermal decomposition of Co_3O_4 to CoO.[54] The SiO_2@α-$Co(OH)_2$ samples (S1, S2 and S3) show weight loss features due to both SiO_2 and α–$Co(OH)_2$ and the overall weight loss values are 25.5 %, 25.2 % and 19.5 %, respectively. The SiO_2@α-$Co(OH)_2$ samples (S1 and S2) show major weight loss (~ 12.5 %) between 30 and 150 °C, while SiO_2@α-$Co(OH)_2$ sample (S3) shows a weight loss of about 4.5 % in the same temperature range. Sample S3 (SiO_2@α–$Co(OH)_2$ prepared using 15 mmol cobalt nitrate) shows different weight loss features compared to S1 and S2 (SiO_2@α–$Co(OH)_2$ samples, prepared using 5 mmol and 10 mmol cobalt nitrate, respectively). It was found from SEM studies (see Figure 4e) that sample S3 before calcination consists of SiO_2@α–$Co(OH)_2$ as well as free α–$Co(OH)_2$ particles. Sample S3 (SiO_2@α–$Co(OH)_2$) shows less weight loss below 150 °C (~ 4.5 %) similar to α–$Co(OH)_2$ (~ 2.5 %). The low weight loss below 150 °C in these samples (α–$Co(OH)_2$ and S3) is attributed to strong interaction between the surface hydroxyl groups which delay the dehydroxylation process.[55,56] The low weight loss at temperature below 150 °C leads to an overall low weight loss in S3. TGA results indicate that the complete formation of spinel Co_3O_4 occurs at about 500 °C by the loss of intercalated water molecules, anions and dehydroxylation of surface hydroxyl groups of α-$Co(OH)_2$.

Morphological studies of the synthesized samples were first investigated using FE-SEM. The FE-SEM images of SiO_2, α-$Co(OH)_2$, and SiO_2@α-$Co(OH)_2$ samples (all the samples before calcination) are shown in Figure 4 (a–e). Pure silica shows uniform spherical particles and the diameter of the spheres is about 300 ± 20 nm; the average diameter of particles and errors were calculated using about ten particles. α-$Co(OH)_2$ consists of sheets and clusters. The SiO_2@α-$Co(OH)_2$ (S1 and S2) show that the silica spheres are completely covered with α–$Co(OH)_2$ sheets (petals) to form a flower–like morphology. But in the case of SiO_2@α-$Co(OH)_2$ sample (S3), the SiO_2 spheres are covered with α–$Co(OH)_2$ sheets and some uncoated particles of α–$Co(OH)_2$ can also be noticed. The FE-SEM images of Co_3O_4 and SiO_2@Co_3O_4 samples (i.e. after calcination) are shown in Figure 5 (a–d). Pure Co_3O_4 shows particles with petals–like morphology. The SiO_2@Co_3O_4 samples (S1 & S2) show uniform shell of Co_3O_4 over the silica core but sample S3 shows coating of Co_3O_4 shell on the SiO_2 spheres with some extra uncoated particulates of Co_3O_4. Based on UV-Vis transmittance measurements, it was found that the dispersion of the core-shell particles in water is stable for at least 6 h. It was also found that the powder obtained after drying the particles can be redispersed effectively.

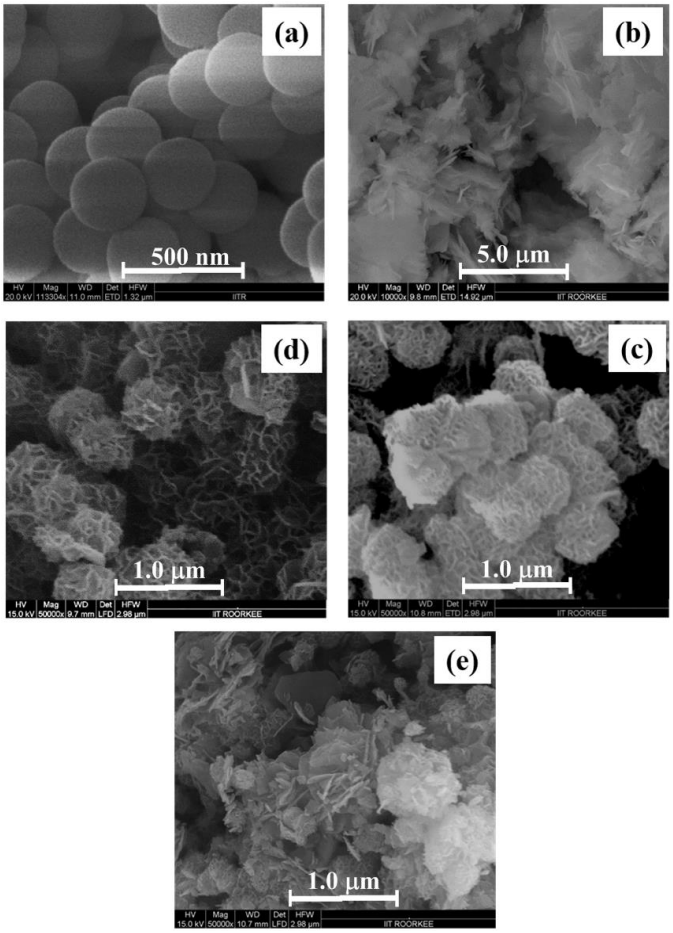

Fig. 4 FE-SEM images of (a) as prepared SiO_2 (b) α-$Co(OH)_2$, and (c–e) SiO_2@α-$Co(OH)_2$ samples.

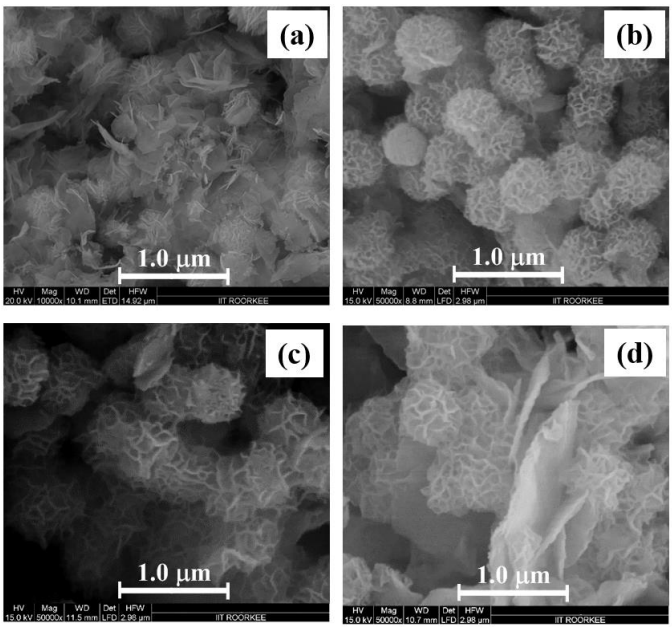

Fig. 5 FE-SEM images of (a) Co_3O_4, and (b–d) SiO_2@Co_3O_4 samples (S1, S2, and S3). All the samples were calcined at 500 °C

Table 1 Elemental composition (Wt. %) of silicon, cobalt, and oxygen in the SiO_2@α-$Co(OH)_2$ and the SiO_2@Co_3O_4 core–shell nanorattles.

Sample name	Weight percent		
	Si	Co	O
SiO_2	28.0 ± 1.4	-	32.5 ± 3.5
α–$Co(OH)_2$	-	93.4 ± 1.5	6.6 ± 1.5
*SiO_2@α-$Co(OH)_2$ (S1)	15.2 ± 1.9	17.6 ± 3.1	37.4 ± 2.3
*SiO_2@α-$Co(OH)_2$ (S2)	13.4 ± 0.2	21.2 ± 2.6	35.1 ± 1.2
*SiO_2@α-$Co(OH)_2$ (S3)	10.9 ± 0.5	23.6 ± 1.5	38.9 ± 1.3
Co_3O_4	-	83.6 ± 0.7	16.4 ± 0.3
SiO_2@Co_3O_4 (S1)	11.1 ± 0.6	14.0 ± 0.5	37.9 ± 0.7
SiO_2@Co_3O_4 (S2)	11.4 ± 0.2	16.0 ± 1.0	34.8 ± 0.1
SiO_2@Co_3O_4 (S3)	9.7 ± 1.1	27.9 ± 0.3	30.3 ± 0.2

*The concentrations of $Co(NO_3)_2.6H_2O$ used during the preparation of SiO_2@α-$Co(OH)_2$ samples S1, S2 and S3 were 5 mM, 10 mM and 15 mM, respectively.

The elemental composition of the SiO_2@α-$Co(OH)_2$ and SiO_2@Co_3O_4 core–shell nanoparticles (S1, S2, and S3) was determined using EDX analysis (Table 1). The EDX results confirm the presence of silicon, oxygen and cobalt in the SiO_2@Co_3O_4 core–shell nanorattles as well as the SiO_2@α-$Co(OH)_2$ samples. Increase in the weight percent of cobalt in the core–shell samples is observed according to the concentration of cobaltous nitrate used during the synthesis of SiO_2@α–$Co(OH)_2$ samples (5 mM, 10 mM, and 15 mM).

The TEM images of SiO_2, Co_3O_4 and SiO_2@Co_3O_4 core–shell samples (S1 & S2) are shown in Figure 6a. TEM analysis was not carried out for the SiO_2@Co_3O_4 sample S3 since the SEM analysis on this sample indicated the presence of uncoated α–$Co(OH)_2$ particles in the SiO_2@α-$Co(OH)_2$ sample (see Figure 4e). SiO_2 shows uniform spherical particles with a diameter of about 300 ± 10 nm. The TEM image indicates the nanosized nature of Co_3O_4 particles (13.7 ± 2.1 nm). The TEM images for the SiO_2@Co_3O_4 samples (S1 & S2) show the core–shell morphology with a void space between the SiO_2 core and the Co_3O_4 shell. These type of structures are referred to as "nanorattles".[24,29] In addition to the nanorattle morphology, the SiO_2@Co_3O_4 samples show porous hair–like morphology for the Co_3O_4 shell. The measured shell thickness values are 37 ± 3 nm, 63 ± 8 nm, for S1 and S2, respectively. The estimated void space between the core and the shell lies between 40 and 45 nm and 64 and 72 nm for the SiO_2@Co_3O_4 samples S1 and S2, respectively. The thickness of hair–like structure of the Co_3O_4 shell was found as 27 ± 3 nm and 45 ± 5 nm for the samples S1 and S2, respectively. The SAED patterns of pure Co_3O_4 and SiO_2@Co_3O_4 core–shell nanorattles (S1 & S2) are shown in Figure 6b. The SAED patterns show spots / rings indicating polycrystalline nature of the samples. The SAED patterns could be indexed to (111), (220), (311), (400), (511), and (440) planes of cubic Co_3O_4. Pure Co_3O_4 exhibits stronger electron diffraction compared to the SiO_2@Co_3O_4 nanorattles (S1 & S2). The less crystalline nature of SiO_2@Co_3O_4 samples compared to pure Co_3O_4 suggest that the Co_3O_4 (shell) particles formed on the silica are smaller in size.

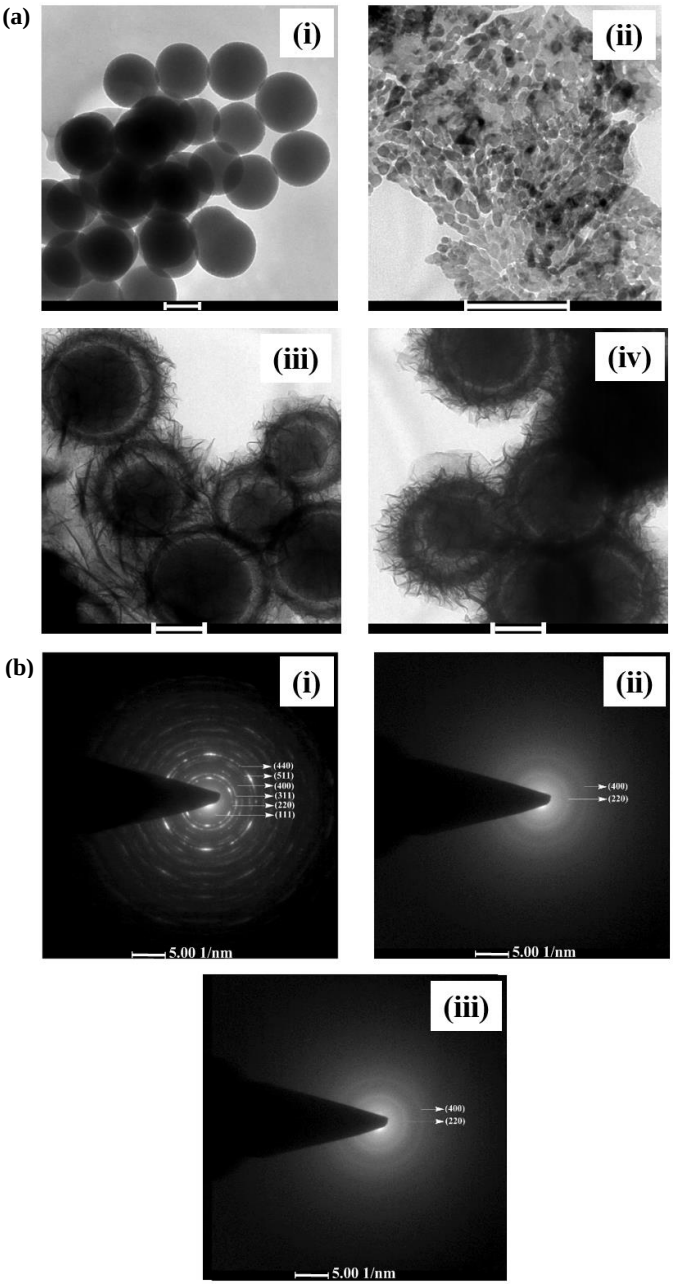

Fig. 6 (a) TEM images of (i) SiO_2, (ii) Co_3O_4, and (iii and iv) SiO_2@Co_3O_4 samples (S1, and S2). The images are obtained for all the samples after calcination at 500 °C. Scale bar is 200 nm. (b) SAED patterns of (i) Co_3O_4, and (ii and iii) SiO_2@Co_3O_4 samples (S1, and S2).

The specific surface area of pure SiO_2, Co_3O_4 and the SiO_2@Co_3O_4 nanorattles (S1 & S2) were measured using Brunauer–Emmett–Teller (BET) measurements using nitrogen

gas physisorption. Pure SiO_2 and Co_3O_4 possess surface area of 34.2 and 46.5 m^2/g, respectively. The $SiO_2@Co_3O_4$ nanorattles (S1 and S2) possess surface area of about 279 m^2/g and 268 m^2/g, respectively. The higher surface area of $SiO_2@Co_3O_4$ nanorattles (S1 and S2) compared to pure Co_3O_4 and SiO_2 is attributed to the nanorattle morphology of $SiO_2@Co_3O_4$ (S1 and S2). The nanorattles consist of porous shell along with the interior void space between the core and the shell.

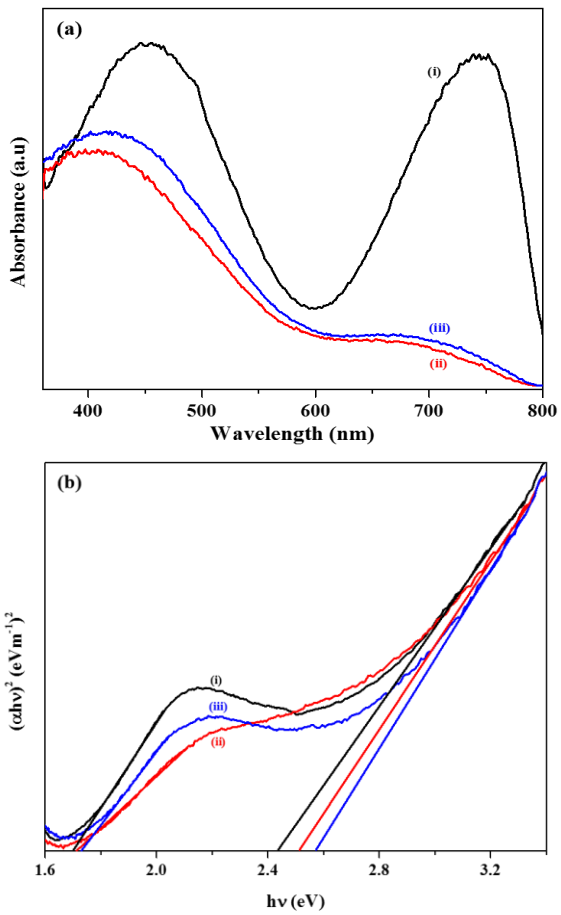

Fig. 7 (a) UV–Vis DRS spectra of (i) Co_3O_4, and (ii and iii) $SiO_2@Co_3O_4$ core–shell nanorattles (S1 and S2). (b) Tauc plots of (i) Co_3O_4, and (ii and iii) $SiO_2@Co_3O_4$ core–shell nanorattles (S1 and S2).

The optical properties of pure Co_3O_4 and $SiO_2@Co_3O_4$ nanorattles (S1 & S2) were studied using UV-Vis diffuse reflectance spectroscopy (Figures 7a & 7b). All the samples exhibit two broad bands in the region 420–450 nm and 700–750 nm. Co_3O_4 shows absorption bands at 745 nm and 450 nm while $SiO_2@Co_3O_4$ samples (S1 & S2) show absorption bands at about 705 nm and 425 nm. The band at 745 nm in pure Co_3O_4 and 705 nm in $SiO_2@Co_3O_4$ samples (S1 & S2) are due to $O^{2-} \rightarrow Co^{3+}$ charge transfer transition and the band at 450 nm in pure Co_3O_4 and 425 nm in $SiO_2@Co_3O_4$ samples (S1 & S2) are due to $O^{2-} \rightarrow Co^{2+}$ charge transfer transition.[19,57] Both the $SiO_2@Co_3O_4$ samples (S1 & S2) show blue shift of about 40 nm with respect to the 745 nm band in pure Co_3O_4 and 25 nm with respect to the 450 nm band in pure Co_3O_4. The blue shift in the case of $SiO_2@Co_3O_4$ samples (S1 & S2) is attributed to quantum confinement effect and smaller particle size of Co_3O_4.[19,57] Co_3O_4 is a p-type semiconductor and the exact band gap energies are calculated using the Tauc equation which can be expressed as $\alpha h\nu = k\,(h\nu - E_g)^n$, where E_g represents the band gap, $h\nu$ is the photon energy, k is the constant, α is the Kubelka-Munk function and n is dependent on the type of transition involved. In the present case, n = 1/2 gives the best fit for $(\alpha h\nu)^{1/n}$ versus photon energy plots suggesting direct allowed transition in Co_3O_4. The calculated band gap energy (E_g) values for Co_3O_4 is 1.70 eV and 2.43 eV and for the $SiO_2@Co_3O_4$ samples, the values were found to be 1.72 eV and 2.52 eV (S1) and 1.74 eV and 2.57 eV (S2). The band gap values for bulk Co_3O_4 are 1.48 eV and 2.19 eV.[58] The obtained band gap values for $SiO_2@Co_3O_4$ samples (S1 & S2) are in good agreement with the previously reported values for Co_3O_4 nanoparticles.[19,59]

3.2 Proposed mechanism for the formation of $SiO_2@Co_3O_4$ core–shell nanorattles

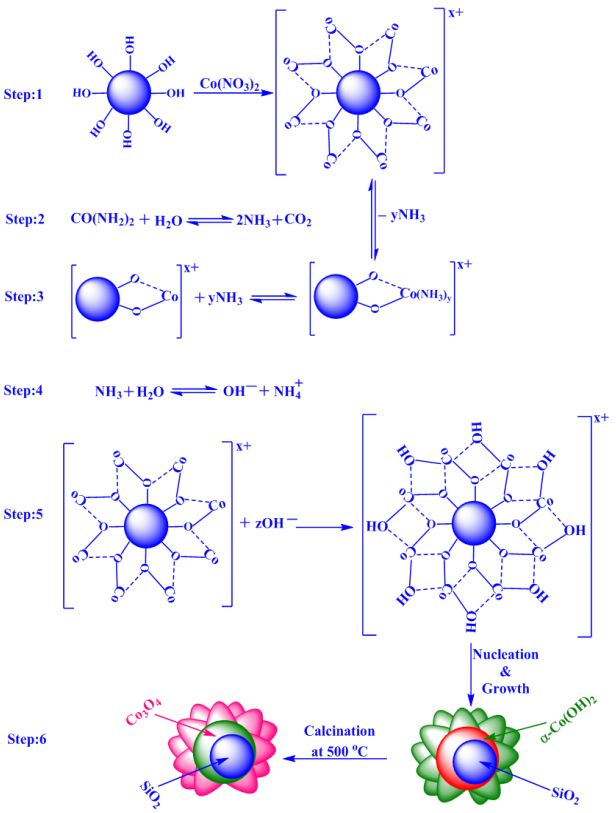

Scheme 1 Proposed mechanism for the formation of $SiO_2@Co_3O_4$ core–shell nanorattles.

For the formation of Co_3O_4 shell on the SiO_2 core, the following mechanism is proposed based on the experimental results (Scheme 1). It is proposed that an adsorption–nucleation –coalescence–anisotropic growth–self–assembly occurs.[60,61] At first, Co^{2+} ions from the solution are adsorbed on the surface of SiO_2 through electrostatic interactions. Urea decomposes to produce NH_3 and CO_2 and the released NH_3 readily reacts with

the available Co^{2+} ions on the surface of SiO_2 to form a complex (i.e. $Co(NH_3)_y$; $y \leq 2$) which reduces the concentration of free Co^{2+} ions in the solution. After attaining the optimum temperature (e.g. 85 °C), OH^- ions are steadily produced through the hydrolysis of urea, which is favorable for nucleation and formation of α–$Co(OH)_2$ on the surface of SiO_2 spheres based on the coalescence mechanism. The α–$Co(OH)_2$ further undergoes Ostwald ripening to produce flower–like hierarchical α–$Co(OH)_2$ on the surface of SiO_2.[61]

Yan et al. and Yuan et al. have explained the formation of hierarchical 3D metal hydroxide flower–like structures based on thermodynamic perspective.[60,61] If one considers a single nanoplatelet of α–$Co(OH)_2$, the surface energy is very high. In order to reduce the overall surface energy, the formed ultrathin α–$Co(OH)_2$ nanoplatlets tend to aggregate which decreases the surface energy by reducing the unsatisfied bonds at the exposed areas. The formed thinner plates self–assemble spontaneously based on the coalescence mechanism to produce thicker plates. The pH would decrease and Ostwald ripening growth would dominate leading to flower–like hierarchical α–$Co(OH)_2$ on the surface of SiO_2. In the final step, calcination of SiO_2@α–$Co(OH)_2$ in air at 500 °C for 3 h leads to the formation of SiO_2@Co_3O_4 core–shell nanorattles through self–template route retaining its 3D hierarchical flower–like morphology for Co_3O_4 nanoparticles.

To understand the mechanism of formation of nanorattle structures further, time dependent TEM analysis (Figure 8) was performed at different time intervals for SiO_2@α-$Co(OH)_2$ (S1) (e.g. 2 h, 4 h and 6h) and SiO_2@Co_3O_4 (e.g. 1 h and 3 h). Initially (e.g. 2 h), α-$Co(OH)_2$ nanoparticles are formed around the SiO_2 spheres (Figure 8a). The crystallites of α-$Co(OH)_2$ present on SiO_2 are loosely packed and the crystallites located at the outermost surface act as the nucleation seeds for the recrystallization process. As the reaction proceeds from 2 h to 4 h, inside-out Ostwald ripening process dominates which starts the hollowing process by dissolving the smaller crystallites of α-$Co(OH)_2$ present in the interior region. At 6 h, the outer α-$Co(OH)_2$ crystallites become larger which creates an interstitial space with the formation of a compact shell. Calcination of SiO_2@α-$Co(OH)_2$ at 500 °C leads to the formation of SiO_2@Co_3O_4 core-shell nanorattles with the retention of core-shell nanorattles morphology (Figure 8b). The TEM images show the shrinkage of silica core as well as the Co_3O_4 shell.

The size of the inner core (SiO_2) and shell (Co_3O_4) particles exhibits a rather larger polydispersity compared to pure SiO_2 and Co_3O_4 particles. This is explained as follows. It can be noted from TEM studies that the formation of an interface between SiO_2 core and α–$Co(OH)_2$ shell occurs within 2 h. After 4 h, formation of core-shell nanorattles with some extra particles of α–$Co(OH)_2$ occurs and core-shell nanorattles with compact α–$Co(OH)_2$ shell are obtained after 6 h. When SiO_2@α–$Co(OH)_2$ core-shell nanorattles are calcined to get the SiO_2@Co_3O_4 core-shell nanorattles, polydispersion of silica core particles with slight shrinkage occurs. Intercalated water molecules and anions (NCO^- and NO_3^-) present in α–$Co(OH)_2$ and surface hydroxyl groups from silica are lost during the conversion of SiO_2@α–$Co(OH)_2$ to SiO_2@Co_3O_4 core-shell nanorattles. The polydispersity of SiO_2 spheres and Co_3O_4 shell is attributed to the different dehydroxylation rate of loss of surface hydroxyl groups and other species from silica (core) and α–$Co(OH)_2$ (shell).

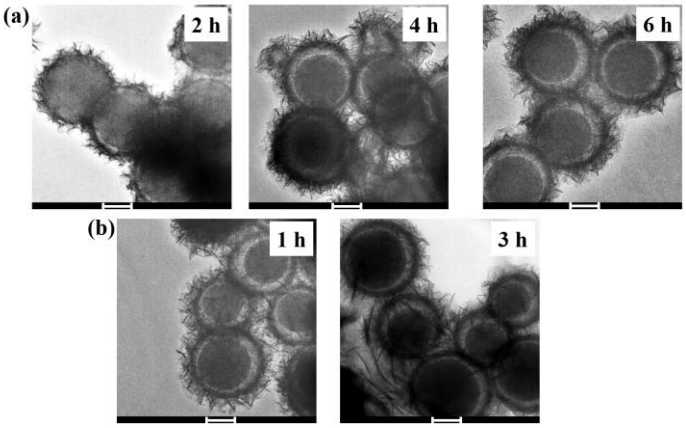

Fig. 8 (a) TEM images of SiO_2@α-$Co(OH)_2$ samples synthesized at 2 h, 4 h and 6 h and (b) the images of SiO_2@Co_3O_4 obtained on calcination of SiO_2@α-$Co(OH)_2$ at 500 °C for 1 h and 3 h. The scale bar is 200 nm.

3.3 The peroxidase–like redox catalytic activity of SiO_2@Co_3O_4 core–shell nanorattles

Enzymes are made up of proteins and they are the active species in bio–catalysis.[7,8] They possess high specificity but they can easily loose their stability in harsh environmental conditions such as high temperature, abnormal pH and in the presence of inhibitors. The lack of stability of natural enzymes provides a chance to explore artificial enzymes in bio–applications. At present, artificial enzymes are very attractive towards bio–catalysis because of their stability and high efficiency under a wide range of temperatures and acidic conditions.[10,34,62]

Horseradish peroxidase (HRP), a natural enzyme, catalyzes the oxidation of substrates (e.g. amines and phenols) in the presence of H_2O_2.[34] Mu et al. and Gao et al. have utilized Co_3O_4[10] and Fe_3O_4 nanoparticles[35] as artificial enzymes for testing the intrinsic peroxidase–like activity towards TMB. Inspired from these reports, peroxidase–like redox activity was examined using the SiO_2@Co_3O_4 core–shell nanorattles (S1, S2 and S3). TMB is a colorless peroxidase substrate which is oxidized by H_2O_2 very slowly to form a blue coloured product. In a typical experiment, the oxidation of TMB was carried out using Co_3O_4 nanoparticles and SiO_2@Co_3O_4 core–shell nanorattles (S1, S2 and S3) as the catalysts in the presence of H_2O_2. The blue colored product formed as a result of the catalytic reaction was monitored by UV–Visible spectroscopy (λ_{max} = 652 nm). A blank reaction was carried out with TMB and H_2O_2 in the absence of any catalyst. It was found that there is no peroxidase activity in the absence of the catalyst which

confirms the role of catalyst in the peroxidase–like activity towards TMB. Although, pure Co_3O_4 nanoparticles and SiO_2@Co_3O_4 core–shell nanorattles (S1, S2 and S3) produce blue coloured product on reaction with TMB in the presence of H_2O_2, the blue colour was more intense in the case of SiO_2@Co_3O_4 core–shell nanorattles (S1, S2 and S3) compared to pure Co_3O_4.

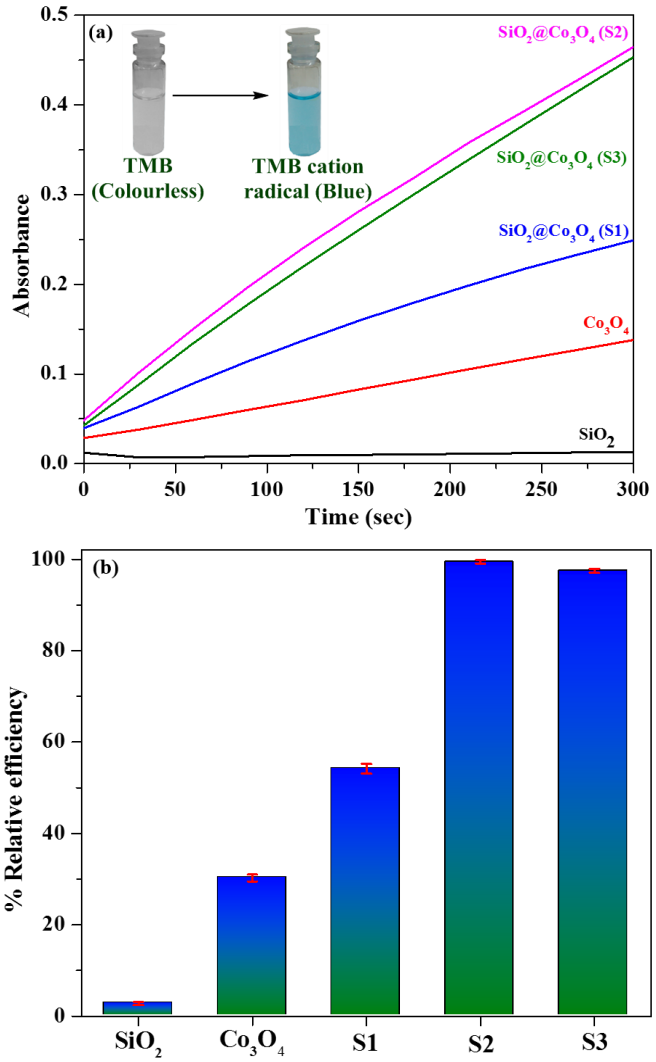

Fig. 9 (a) Time dependent UV–Visible spectral results indicating the peroxidase–like activity on TMB using SiO_2, Co_3O_4, and SiO_2@Co_3O_4 core–shell nanorattles (S1, S2 and S3) as the catalyst (λ_{max} = 652 nm). (b) Comparison of peroxidase activity of SiO_2@Co_3O_4 core–shell nanorattles (S1, S2 and S3) with that of SiO_2 and Co_3O_4 nanoparticles.

The time dependent catalytic activity for Co_3O_4 and SiO_2@Co_3O_4 core–shell nanorattles towards TMB oxidation, as indicated by UV–Visible spectral results are shown in Figure 9(a). Their relative catalytic efficiency is shown in Figure 9(b) which follows the order: S2 > S3 > S1 > Co_3O_4 > SiO_2. The activity of sample S3 is lower compared to S2 but higher than that of S1 (Figure 9a).

3.4 Effect of physicochemical conditions on the peroxidase-like activity

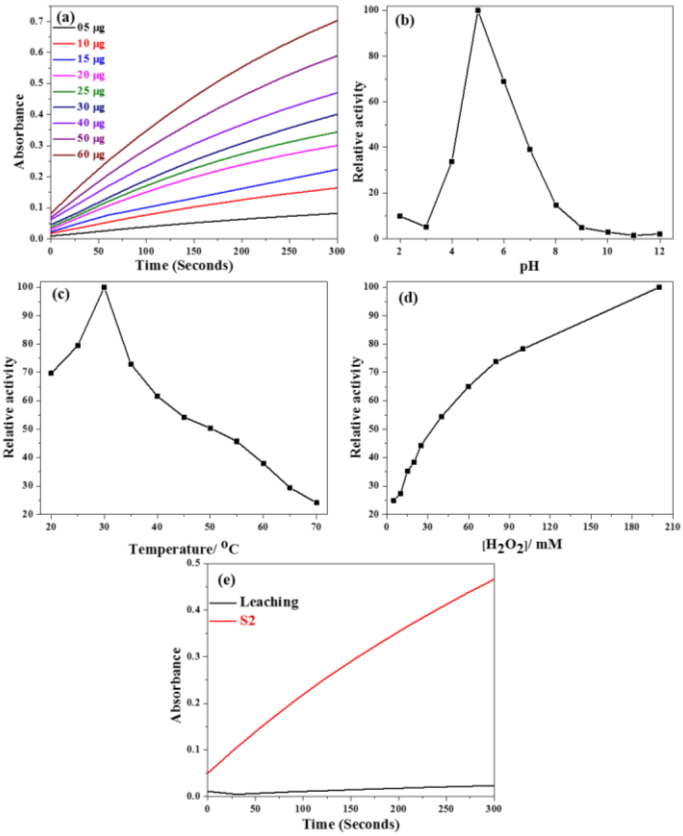

Fig. 10 The effect of physicochemical conditions on peroxidase–like activity of SiO_2@Co_3O_4 core–shell nanorattles (S2): (a) amount of catalyst, (b) pH, (c) temperature, (d) H_2O_2 concentration, and (e) the effect of leaching.

Any catalytic reaction demands optimum conditions for maximum activity. In the present study, TMB and H_2O_2 were chosen as the reagents. Effort was made to understand the catalytic activity of SiO_2@Co_3O_4 core–shell nanorattles on various conditions such as amount of the catalyst, temperature, and pH. The amount of catalyst (SiO_2@Co_3O_4, S2) was varied from 5 μg to 60 μg per 3 mL while keeping the pH of acetate buffer at 5, temperature at 30 °C and the concentration of H_2O_2 at 100 mM. A linear relationship between the amount of catalyst and peroxidase activity was found (Figure 10a). The catalytic activity was tested by varying the pH from 2 to 12 and also by varying the temperature between 20 and 70 °C while keeping the amount of catalyst (SiO_2@Co_3O_4, S2) at 30 μg per 3 mL, and the concentration of TMB and H_2O_2 at 0.3 mM and 100 mM, respectively. From the results (Figures 10b and 10c), the optimized pH and temperature were found as 5 and 30 °C, respectively. The effect of H_2O_2 concentration on the catalytic activity of SiO_2@Co_3O_4 (S2) was also studied. By increasing the H_2O_2 concentration, the peroxidase–like activity of the SiO_2@Co_3O_4 core-shell nanorattles is steady even at higher H_2O_2 concentrations (Figure 10d). Previous reports have indicated that higher concentration of H_2O_2 exhibits negative

impact on the activity. At higher concentrations, H_2O_2 inhibits the catalytic activity of HRP due to its conversion from active form to an inactive form.[10,63] Leaching test was also performed to prove that the peroxidase–like activity of the catalysts does not result from the leaching of cobalt ions from the catalysts into the solution. To prove this, 30 μg of $SiO_2@Co_3O_4$ (S2) was incubated in 3 mL of acetate buffer solution (pH = 5) for 30 minutes, and then the $SiO_2@Co_3O_4$ sample was separated from the buffer solution by centrifugation. The catalytic activity using the resultant solution (from the leaching) was tested (3 mL of solution, 300 µL of 3 mM TMB, and 31 µL of 100 mM H_2O_2). The peroxidase activity using the leached solution was compared with that of $SiO_2@Co_3O_4$ sample (S2). Negligible absorbance was found as shown in Figure 10 (e) when the leached solution was used as the catalyst. These results conclude that the peroxidase–like activity is only due to Co_3O_4 nanoparticles and not from the leached cobalt ions.

3.5 Steady–state kinetic studies using $SiO_2@Co_3O_4$ core–shell nanorattles

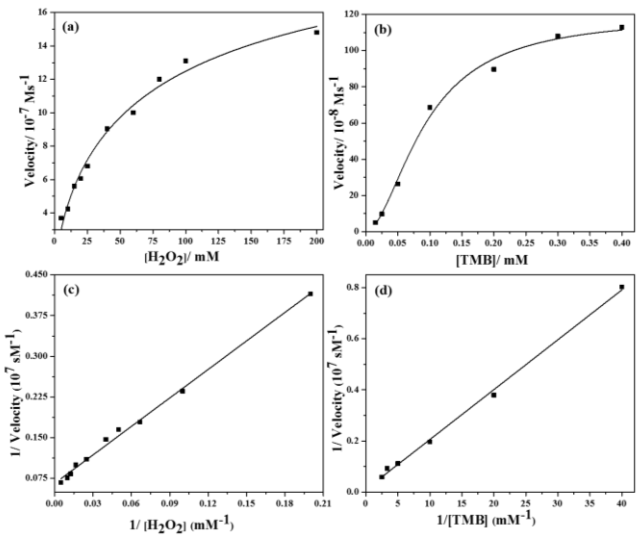

Fig. 11 Steady state kinetic analysis for $SiO_2@Co_3O_4$ core–shell nanorattles (S2) under various conditions: (a) [TMB] = 0.3 mM; [H_2O_2] = 20–200 mM, (b) [H_2O_2] = 100 mM; [TMB] = 0.015–0.4 mM, and (c & d) are the Lineweaver–Burk double reciprocal plots corresponding to conditions (a) and (b). Other conditions: 30 µg catalyst per 3 mL of 0.1 M acetate buffer, pH = 5, and temperature = 30 °C.

To understand the peroxidase–like activity of $SiO_2@Co_3O_4$ core–shell nanorattles better, steady state kinetic analysis was carried out by choosing TMB and H_2O_2 as the reactants. The kinetic analysis was carried out by varying the concentration of TMB while keeping the H_2O_2 concentration constant, and vice-versa (Figure 11). The steady state kinetic parameters (Michaelis constant, K_m and maximal reaction velocity, V_{max}) were estimated using the Lineweaver–Burk double reciprocal plots[9,42] which show linear relationship between 1/[V] and 1/[S], as shown in Figures 11c and 11d. The estimated kinetic parameters for the $SiO_2@Co_3O_4$ core–shell nanorattle (S2) were compared with that of Co_3O_4 nanoparticles and HRP (Table 2).

The Michaelis constant (K_m), obtained from the slope of Lineweaver–Burk double reciprocal plot, is related to properties of the substrate, enzyme and the reaction conditions.[9] A smaller K_m value indicates higher affinity between the substrate and the enzyme. The K_m value for $SiO_2@Co_3O_4$ core–shell nanorattles (S2) is 0.085 for TMB and 24.29 for H_2O_2, respectively. The K_m values for TMB and H_2O_2 are comparable with that of Co_3O_4–carbon nitride nanotubes[42] (0.056 for TMB and 30.04 for H_2O_2) and Co_3O_4/reduced graphene oxide (0.19 for TMB and 24.04 for H_2O_2).[43] The obtained results were compared with the literature values for pure Co_3O_4 nanoparticles and HRP.[10,62] The $SiO_2@Co_3O_4$ core–shell nanorattles (S2) exhibit five times higher affinity for TMB than HRP and almost two times lower affinity for TMB compared to pure Co_3O_4 nanoparticles. In the case of H_2O_2, the $SiO_2@Co_3O_4$ core–shell nanorattles (S2) show almost six times higher affinity compared to Co_3O_4 nanoparticles and six times lower affinity compared to HRP. Higher concentration of H_2O_2 and lower concentration of TMB are the best conditions to achieve maximum peroxidase–like activity using the $SiO_2@Co_3O_4$ core–shell nanorattles. The higher activity of the nanorattles compared to HRP is attributed to the availability of more active sites on the surface of $SiO_2@Co_3O_4$ core–shell nanorattles compared to HRP, which has only one active site (iron (II)).[35,62]

In order to compare the peroxidase–like activity of $SiO_2@Co_3O_4$ core–shell nanorattles (S2) with that of natural peroxidase (HRP) and pure Co_3O_4 nanoparticles, k_{cat} values were also estimated (Table 2). The k_{cat} value for $SiO_2@Co_3O_4$ core–shell nanorattles (S2) is much higher than that of pure Co_3O_4 and HRP. These results suggest that the $SiO_2@Co_3O_4$ core–shell nanorattles (S2) can be used as highly efficient peroxidase mimic compared to pure Co_3O_4 nanoparticles and HRP.[10,62] The ratio of k_{cat}/K_m is often referred to as specificity constant; a higher specificity constant value indicates higher peroxidase–like activity of the material. The k_{cat}/K_m values estimated for $SiO_2@Co_3O_4$ core–shell nanorattles (S2) are given in Table 2. In the present study, the $SiO_2@Co_3O_4$ core–shell nanorattles show higher specificity constant compared to pure Co_3O_4 and HRP for TMB. With respect to H_2O_2, the $SiO_2@Co_3O_4$ core–shell nanorattles (S2) show two orders of magnitude higher specificity compared to pure Co_3O_4 nanoparticles and the specificity is similar to that of HRP.[62] These results demonstrate that the $SiO_2@Co_3O_4$ core–shell nanorattles show higher peroxidase–like activity compared to Co_3O_4 nanoparticles and HRP.

3.6 Proposed mechanism for the peroxidase–like activity on TMB using $SiO_2@Co_3O_4$ core–shell nanorattles

The proposed mechanism for the peroxidase–like activity of $SiO_2@Co_3O_4$ core–shell nanorattles on TMB is given in Scheme 2.[10,42,43]

Table 2 Comparison of the kinetic parameters for $SiO_2@Co_3O_4$ core–shell nanorattles with those for Co_3O_4 and HRP

Catalyst	*[E]/ M	Substrate	K_m /mM	V_{max}/ Ms^{-1} (10^{-8})	k_{cat}/ s^{-1}	k_{cat}/K_m ($M^{-1}s^{-1}$)	Reference
$SiO_2@Co_3O_4$ (S2)	7.54×10^{-11}	TMB	0.087±0.0028	0.012±0.00056	1.49×10^4	1.75×10^8	Present work
$SiO_2@Co_3O_4$ (S2)	7.54×10^{-11}	H_2O_2	25.2±1.28	0.015±0.00035	1.96×10^4	8.08×10^5	Present work
Co_3O_4	3.43×10^{-10}	TMB	0.037	6.27	1.83×10^2	4.94×10^6	[1]
Co_3O_4	3.43×10^{-10}	H_2O_2	140.07	12.1	3.53×10^2	2.52×10^3	″
HRP	2.50×10^{-11}	TMB	0.434	10.0	4.00×10^3	9.22×10^6	[2]
HRP	2.50×10^{-11}	H_2O_2	3.70	8.71	3.48×10^3	9.40×10^5	″

* [E] = The concentration of catalyst (e.g. $SiO_2@Co_3O_4$) or the concentration of enzyme (HRP).

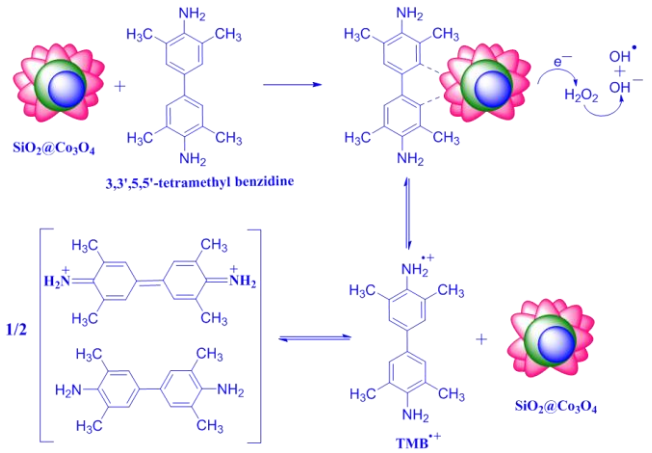

Scheme 2 Proposed mechanism for the peroxidase–like activity on TMB using $SiO_2@Co_3O_4$ core–shell nanorattles.

Neither H_2O_2 nor $SiO_2@Co_3O_4$ core-shell nanorattles alone was found to exhibit the peroxidase-like activity. The presence of $SiO_2@Co_3O_4$ and H_2O_2 together are important for the peroxidase-like activity on tetramethyl benzidine. When $SiO_2@Co_3O_4$, H_2O_2 and TMB are present, the TMB molecules adsorb on the surface of $SiO_2@Co_3O_4$ and increases the electron density by donating the lone pair electrons of the amino groups.[10,64] XPS or WAXS measurements would give more evidence on this aspect and this would be part of future studies. The $SiO_2@Co_3O_4$ core-shell nanorattles induce electrochemical reduction of H_2O_2 producing OH^- and $OH^\bullet$ species which involve in the oxidation of TMB to produce $TMB^{\bullet+}$ (a charge transfer complex which is blue in color). Mu et al. have reported the electrochemical reduction of H_2O_2 using pure Co_3O_4 nanoparticles.[10] In the case of core-shell nanorattles, there is an assembly of Co_3O_4 nanoparticles on the surface of SiO_2 spheres. The TMB molecules undergo less steric hindrance to reach the catalytic active centers (cobalt) in the case of $SiO_2@Co_3O_4$ core-shell nanorattles compared to pure Co_3O_4 nanoparticles. This increases the electron density on the core-shell nanorattles and facilitate the electron transfer. The enhancement in the peroxidase-like activity of $SiO_2@Co_3O_4$ core-shell nanorattles compared to pure Co_3O_4 nanoparticles is due to increased surface area and also due to increase in the electron density in the case of $SiO_2@Co_3O_4$ core-shell nanorattles compared to pure Co_3O_4 nanoparticles. Sample S2 shows higher activity than S1 and this is due to the presence of more number of catalytic active centers in S2 compared to S1 but sample S3 consists of free Co_3O_4 nanoparticles in addition to $SiO_2@Co_3O_4$ nanorattles which leads to lower activity compared to S2.

4. Conclusions

A novel self–template method for the synthesis of $SiO_2@Co_3O_4$ core–shell nanorattles with different shell thickness has been reported. Compared to other preparation methods, this approach does not require any surface modification and the method is facile, and inexpensive. The synthesized $SiO_2@Co_3O_4$ core–shell nanorattles were characterized using a variety of techniques. The $SiO_2@Co_3O_4$ core–shell nanorattles possess enhanced intrinsic peroxidase–like activity compared to pure Co_3O_4 nanoparticles and HRP and it follows Michaelis–Menten kinetics. The enhanced peroxidase–like activity of $SiO_2@Co_3O_4$ core–shell nanorattles is due to the synergistic interaction between the SiO_2 core and the Co_3O_4 shell. The nanorattles show higher k_{cat} and k_{cat}/K_m values compared to pure Co_3O_4 nanoparticles and HRP suggesting their applicability as an artificial enzyme mimic in biomedicine and bio–sensing applications.

Acknowledgements

Syam Kandula thanks the Ministry of Human Resources and Development (MHRD), Govt. of India for the financial support. The authors are thankful to the Institute Instrumentation Centre, IIT Roorkee for providing the facilities.

Notes and references

Department of Chemistry, Indian Institute of Technology Roorkee, Roorkee–247667, India

** E-mail: jeevafcy@iitr.ac.in Tel: +91–1332–285444; Fax: 91–1332 –273560*

Electronic Supplementary Information (ESI) available: Overview image of SiO_2@Co_3O_4 core-shell nanorattles. See DOI: 10.1039/b000000x/

1 X. Xu, B. Tian, J. Kong, S. Zhang, B. Liu and D. Zhao, *Adv. Mater.*, 2003, **15**, 1932-1936.
2 W. Shi, X. Zhang, S. He and Y. Huang, *Chem. Commun.*, 2011, **47**, 10785-10787.
3 W. Chen, J. Chen, Y. B. Feng, L. Hong, Q. Y. Chen, L. F. Wu, X. H. Lin and X. H. Xia, *Analyst*, 2012, **137**, 1706-1712.
4 L. Zhang, L. Han, P. Hu, L. Wang and S. Dong, *Chem. Commun.*, 2013, **49**, 10480-10482.
5 C. Ray, S. Dutta, S. Sarkar, R. Sahoo, A. Roy and T. Pal, *J. Mater. Chem. B*, 2014, **2**, 6097-6105.
6 G. Nie, L. Zhang, J. Lei, L. Yang, Z. Zhang, X. Lu and C. Wang, *J. Mater. Chem. A*, 2014, **2**, 2910-2914.
7 W. Zhang, X. Liu, D. Walsh, S. Yao, Y. Kou and D. Ma, *Small*, 2012, **8**, 2948-2953.
8 J. Dong, L. Song, J. J. Yin, W. He, Y. Wu, N. Gu and Y. Zhang, *ACS Appl. Mater. Interfaces*, 2014, **6**, 1959-1970.
9 H. Sun, X. Jiao, Y. Han, Z. Jiang and D. Chen, *Eur. J. Inorg. Chem.*, 2013, **2013(1)**, 109-114.
10 J. Mu, Y. Wang, M. Zhao and L. Zhang, *Chem. Commun.*, 2012, **48**, 2540-2542.
11 B. J. Jankiewicz, D. Jamiola, J. Choma and M. Jaroniec, *Adv. Colloid Interface Sci.*, 2012, **170**, 28-47.
12 Y. Piao, A. Burns, J. Kim, U. Wiesner and T. Hyeon, *Adv. Funct. Mater.*, 2008, 18, 3745-3758.
13 C. G. Schaefer, S. Vowinkel, G. P. Hellmann, T. Herdt, C. Contiu, J. J. Schneider and M. Gallei, *J. Mater. Chem. C*, 2014, 2, 7960-7975.
14 L. Ren, P. Wang, Y. Han, C. Hu and B. Wei, *Chem. Phys. Lett.*, 2009, **476**, 78-83.
15 Y. Kim, J. H. Lee, S. Cho, Y. Kwon, I. In, J. Lee, N. H. You, E. Reichmanis, H. Ko, K. T. Lee, H. K. Kwon, D. H. Ko, H. Yang and B. Park, *ACS Nano*, 2014, **8**, 6701-6712.
16 C. Sun, S. Rajasekhara, Y. Chen and J. B. Goodenough, *Chem. Commun.*, 2011, **47**, 12852-12854.
17 X. Wang, X. Chen, L. Gao, H. Zheng, Z. Zhang and Y. Qian, *J. Phys. Chem. B*, 2004, **108**, 16401-16404.
18 E. Barrera, I. Gonzalez and T. Viveros, *Sol. Energy Mater. Sol. Cells*, 1998, **51**, 69-82.
19 K. Deori, S. K. Ujjain, R. K. Sharma and S. Deka, *ACS Appl. Mater. Interfaces*, 2013, **5**, 10665-10672.
20 J. D. Blakemore, H. B. Gray, J. R. Winkler and A. M. Muller, *ACS Catal.*, 2013, **3**, 2497-2500.
21 N. Kang, J. H. Park, M. Jin, N. Park, S. M. Lee, H. J. Kim, J. M. Kim and S. U. Son, *J. Am. Chem. Soc.*, 2013, **135**, 19115-19118.
22 N. Yan, Q. Chen, F. Wang, Y. Wang, H. Zhong and L. Hu, *J. Mater. Chem. A*, 2013, **1**, 637-643.
23 L. Tan, X. Wu, D. Chen, H. Liu, X. Meng and F. Tang, *J. Mater. Chem. A*, 2013, **1**, 10382-10388.
24 P. Yang, F. Wang, X. Luo, Y. Zhang, J. Guo, W. Shi and C. Wang, *ACS Appl. Mater. Interfaces*, 2014, **6**, 12581-12587.
25 B. Zhang, T. Cai, S. Li, X. Zhang, Y. Chen, K. G. Neoh, E. T. Kang and C. Wang, *J. Mater. Chem. C*, 2014, **2**, 5189-5197.
26 X. Liang, J. Li, J. B. Joo, A. Gutierrez, A. Tillekaratne, I. Lee, Y. Yin and F. Zaera, *Angew. Chem. Int. Ed.*, 2012, **51**, 8034-8036.
27 P. H. C. Camargo, Z. Y. Li and Y. Xia, *Soft Matter*, 2007, **3**, 1215-1222.
28 D. Scheid, G. Cherkashinin, E. Ionescu and M. Gallei, *Langmuir*, 2014, **30**, 1204-1209.
29 J. Xu, J. Liu, R. Che, C. Liang, M. Cao, Y. Li and Z. Liu, *Nanoscale*, 2014, **6**, 5782-5790.
30 W. Na, Q. Wei and Z. Nie, *J. Mater. Chem.*, 2012, **22**, 9970-9974.
31 A. Agiral, H. S. Soo and H. Frei, *Chem. Mater.*, 2013, **25**, 2264-2273.
32 R. Xie, C. Wang, L. Xia, H. Wang, T. Zhao and Y. Sun, *Catal. Lett.*, 2014, **144**, 516-523.
33 J. Zong, Y. Zhu, X. Yang and C. Li, *J. Alloys Compd.*, 2011, **509**, 2970-2975.
34 J. Mu, L. Zhang, G. Zhao and Y. Wang, *Phys. Chem. Chem. Phys.*, 2014, **16**, 15709-15716.
35 L. Gao, J. Zhuang, L. Nie, J. Zhang, Y. Zhang, N. Gu, T. Wang, J. Feng, D. Yang, S. Perrett and X. Yan, *Nat. Nanotechnol.*, 2007, **2**, 577-583.
36 H. Chen, Y. Li, F. Zhang, G. Zhang and X. Fan, *J. Mater. Chem.*, 2011, **21**, 17658-17661.
37 X. Chen, X. Tian, B. Su, Z. Huang, X. Chen and M. Oyama, *Dalton Trans.*, 2014, **43**, 7449-7454.
38 L. Chen, B. Sun, X. Wang, F. Qiao and S. Ai, *J. Mater. Chem. B*, 2013, **1**, 2268-2274.
39 K. Cai, Z. Lv, K. Chen, L. Huang, J. Wang, F. Shao, Y. Wang and H. Han, *Chem. Commun.*, 2013, **49**, 6024-6026.
40 G. Nie, L. Zhang, X. Lu, X. Bian, W. Sun and C. Wang, *Dalton Trans.*, 2013, **42**, 14006-14013.
41 H. Wang, S. Li, Y. Si, Z. Sun, S. Li and Y. Lin, *J. Mater. Chem. B*, 2014, **2**, 4442-4448.
42 C.O. Song, J. W. Lee, H. S. Choi and J. K. Jeung, *RSC. Adv.*, 2013, **3**, 20179-20185.
43 J. Xie, H. Cao, H. Jiang, Y. Chen, W. Shi, H. Zheng and Y. Huang, *Anal. Chim. Acta*, 2013, **796**, 92-100.
44 S. Kandula and P. Jeevanandam, *J. Alloys Compd.*, 2014, **615**, 167-176.
45 Z. Liu, R. Ma, M. Osada, K. Takada and T. Sasaki, *J. Am. Chem. Soc.*, 2005, **127**, 13869-13874.
46 W. Chen, Y. Yang, H. Shao and J. Fan, *J. Phys. Chem. C*, 2008, **112**, 17471-17477.
47 J. P. Cheng, L. Liu, J. Zhang, F. Liu and X. B. Zhang, *J. Electroanal. Chem.*, 2014, **722-723**, 23-31.
48 Q. Wang, S. Liu, H. Sun and Q. Lu, *Ind. Eng. Chem. Res.*, 2014, **53**, 7917-7922.
49 Y. Oaki, S. Kajiyama, T. Nishimura and T. Kato, *J. Mater. Chem.*, 2008, **18**, 4140-4142.
50 P. N. R. Kishore and P. Jeevanandam, *J. Nanosci. Nanotechnol.*, 2013, **13**, 2908-2916.
51 R. L. Frost, D. L. Wain, W. N. Martens and B. J. Reddy, *Spectrochim. Acta Mol. Biomol. Spectros.*, 2007, **66A**, 1068-1074.
52 N. Bayal and P. Jeevanandam, *J. Nanopart. Res.*, 2013, **15**, 2066/1-15.
53 D. Ghosh, S. Giri and C. K. Das, *ACS Sustainable Chem. Eng.*, 2013, **1**, 1135-1142.
54 Z. Z. Xu, Z. L. Chen, Y. Ben and J. M. Shen, *Mater. Lett.*, 2009, **63**, 1210-1212.
55 S. J. Palmer, R. L. Frost and T. Nguyen, *Coord. Chem. Rev.*, 2009, **253**, 250-267.

56 F. Malherbe and J. P. Besse, *J. Solid State Chem.*, 2000, **155**, 332-341.
57 K. Deori and S. Deka, *CrystEngComm*, 2013, **15**, 8465-8474.
58 S. Farhadi, K. Pourzare and S. Bazgir, *J. Alloys Compd.*, 2014, **587**, 632-637.
59 A. Gulino, P. Dapporto, P. Rossi and I. Fragala, *Chem. Mater.*, 2003, **15**, 3748-3752.
60 J. Yan, Z. Fan, W. Sun, G. Ning, T. Wei, Q. Zhang, R. Zhang, L. Zhi and F. Wei, *Adv. Funct. Mater.*, 2012, **22**, 2632-2641.
61 C. Yuan, X. Zhang, L. Su, B. Gao and L. Shen, *J. Mater. Chem.*, 2009, **19**, 5772-5777.
62 X. Q. Zhang, S. W. Gong, Y. Zhang, T. Yang, C. Y. Wang and N. Gu, *J. Mater. Chem.*, 2010, **20**, 5110-5116.
63 J. A. Nicell and H. Wright, *Enzyme Microb. Technol.*, 1997, **21**, 302-310.
64 Y. Song, K. Qu, C. Zhao, J. Ren and X. Qu, *Adv. Mater.*, 2010, **22**, 2206-2210.

Table of Contents entry

A Facile Synthetic Approach for $SiO_2@Co_3O_4$ Core–Shell Nanorattles with Enhanced Peroxidase–Like Activity

Syam Kandula and Pethaiyan Jeevanandam*

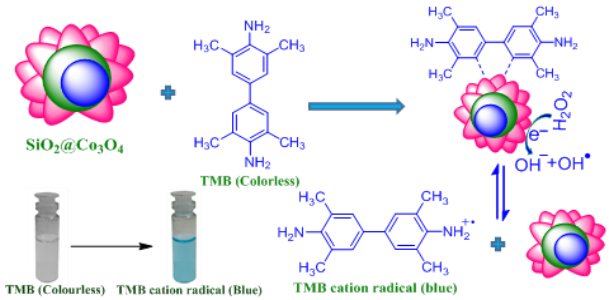

$SiO_2@Co_3O_4$ core–shell nanorattles have been successfully synthesized through a novel self–template route by the calcination of $SiO_2@\alpha$-$Co(OH)_2$ at 500 ºC and the nanorattles exhibit enhanced peroxidase–like activity.